Microporous and Mesoporous Materials 125 (2009) 11–16

Contents lists available at ScienceDirect

Microporous and Mesoporous Materials

journal homepage: www.elsevier.com/locate/micromeso

Diffusion of *n*-butane/*iso*-butane mixtures in silicalite-1 investigated using infrared (IR) microscopy

C. Chmelik [a,*], L. Heinke [a], J.M. van Baten [b], R. Krishna [b]

[a] Department of Interface Physics, University of Leipzig, Linnéstrasse 5, D-04103 Leipzig, Germany
[b] Van't Hoff Institute for Molecular Sciences, University of Amsterdam, Nieuwe Achtergracht 166, 1018 WV Amsterdam, The Netherlands

ARTICLE INFO

Article history:
Received 25 November 2008
Received in revised form 30 January 2009
Accepted 3 February 2009
Available online 20 February 2009

Keywords:
Diffusion
Butane
Mixture
IR microscopy
Configurational Bias Monte-Carlo
MFI
Silicalite-1

ABSTRACT

Adsorption and diffusion of *n*-butane/*iso*-butane mixtures in individual silicalite-1 crystals has been investigated using infrared (IR) microscopy. The equilibrium sorption isotherm for an equimolar gas phase mixture is calculated using Configurational Bias Monte-Carlo simulations. The comparison between simulation results and the experimental data enabled the determination of absolute values of concentration in the IR experiments.

n-Butane uptake under presence of *iso*-butane and, vice versa, *iso*-butane uptake under presence of *n*-butane have been studied experimentally. It is shown that the *n*-butane counter-uptake is not limited by the *n*-butane diffusivity, but by the availability of free sites, which is, in turn, determined by the mobility of *iso*-butane. A site-percolation threshold, given by the number of *iso*-butane molecules blocking the 'traffic junctions' of the channel network, has been employed for explaining the occurrence of network regions which are initially inaccessible for *n*-butane in the counter-uptake process.

1. Introduction

Professor Jörg Kärger is one of the true pioneers of studying molecular transport in zeolites and other nanoporous solids. With his work and leadership two particular powerful experimental techniques for diffusion measurements have been developed at the University of Leipzig, namely NMR with pulsed field gradients (PFG NMR) and interference microscopy. Professor Kärger has published and co-authored about 450 papers devoted to diffusion of single components and mixtures [1–5] in nanoporous materials.

In the past 30 years especially PFG NMR provided new and deep insights in the microdynamics of molecular transport by numerous studies using this technique. Moreover, it also initialized the development and application of several new experimental techniques, which emerged in response to PFG NMR diffusion measurements [6]. However, also interference microscopy has been presented to the community as very powerful tool for investigating molecular transport on a microscopic scale in the recent years [7–10]. Now, following the pioneering work by Helmut Karge [11–14], also diffusion measurements using infrared (IR) microscopy are pursued in the Leipzig group. One of the main advances of the IR microscopy technique is the ability to differentiate between different sorbates and allows in this way studies of mixture diffusion in zeolites and other nanoporous materials.

Zeolites are widely used as catalysts and adsorbents in applied chemistry and technology. Practically all important applications in adsorption, separation and catalysis involve mixtures. However, due to the experimental difficulty, the number of experimental studies of mixture adsorption and diffusion is rather small compared to single components. Nevertheless, different experimental techniques have been applied to study aspects of mixture diffusion, e.g. PFG NMR [1–5,15], QENS [16], tracer-exchange positron emission profiling [17], IR spectroscopy [11–14] and membrane permeation [18,19,20].

Zeolites of MFI-type belong to the most important zeolite structures in catalysis and are used in many shape-selective processes in petroleum refining industry, in particular for the adsorptive separation of alkane isomers [21–23]. Recently, the influence of intersection blocking by branched and cyclic hydrocarbons on diffusion of hydrocarbon mixtures in MFI zeolites has been studied using molecular dynamic simulations [24]. Motivated by the practical relevance, as model system we considered a mixture of a linear and mono-branched alkanes, viz. *n*-butane (nC4) and *iso*-butane (iC4), in MFI zeolites. To our knowledge, here we present the first results of mixture diffusion measured in individual zeolite crystals.

Recently, the self-diffusivity of nC4 under presence of iC4 has been examined using PFG NMR in combination with molecular simulations [5]. In our present work, we present results of mixture adsorption and diffusion in single MFI crystals measured with IR microscopy. This includes in particular the qualitative interpretation of the uptake of nC4 under presence of iC4 (and vice versa),

* Corresponding author. Tel.: +49 341 9732531; fax: +49 341 9732549.
E-mail address: chmelik@physik.uni-leipzig.de (C. Chmelik).

1387-1811/$ - see front matter © 2009 Elsevier Inc. All rights reserved.
doi:10.1016/j.micromeso.2009.02.015

i.e. of molecular transport under non-equilibrium conditions. Configurational Bias Monte-Carlo (CBMC) simulations of adsorption equilibrium are used to aid the interpretation of the experimental data.

2. Materials and methods

The main points of the IR microscopy technique and the experimental setup are given below. Further details are described elsewhere [25,26].

The experimental setup consists of a static vacuum system attached to an IR microscope. Prior to the measurement, a few crystals were introduced into the IR cell and activated. For the measurement only one individual zeolite crystals is selected using the aperture and motorized sample platform of the microscope. The investigated crystals were approximately $25 \times 25 \times 180\ \mu m^3$ in size. To follow the uptake of the guest molecules within the crystal, absorption spectra were recorded in the IR-transmission mode of the microscope with a temporal resolution between 0.2 and 1.5 s. Following the Beer–Lambert law, the absorbance of characteristic IR bands is assumed to be proportional to the concentration of guest molecules. To differentiate between nC4 and iC4 in the mixture, nC4 has been used in its fully deuterated form (degree of deuteration > 99%). For calculating the respective intracrystalline concentration the area under the C–H or C–D stretching vibrations have been determined, respectively. Uptake or release experiments are initialized by step-changes in the gas phase surrounding the crystals. In the case of nC4 counter-adsorption the iC4 atmosphere was rapidly replaced by nC4. All experiments were carried out at room temperature, i.e. at 298 K.

IR spectroscopy has been employed for mixture experiments in zeolites for the first time about 20 years ago by Karge and Weitkamp [11]. Later, Karge and Nießen published a systematic study of co- and counter-diffusion of binary mixtures of benzene, ethylbenzene and *p*-xylene in MFI-type zeolites [12–14]. Two main differences to our experiments shall be pointed out. (i) We investigate only one individual crystal instead a batch or self-supporting wafers. (ii) We operate with a static vacuum system, i.e. without carrier gas or continuous gas flow.

Beside the ability to investigate differences between different individual crystals, another important benefit of our system is that changes in the gas phase surrounding the crystals occur almost instantaneously and do not require functions correcting for time-lag effects introduced by finite flow rates. By measuring the gas phase concentration directly beside crystals it was found that pressure steps are equilibrated in less than 0.2 s, marking the absence of valve effects [27]. As shown later, this may even allow conclusions for mixture systems where the typical time constant of the fast component is smaller than 1 s. However, for the mixture experiments it is essential to ensure that: (i) the volume of the vacuum cell is large compared to the amount adsorbed by the crystals inside the cell, and (ii) that limitations by gas transport through stagnant gas layers [28] can be excluded. Influences as the latter may occur in our setup in mixture desorption steps other than to vacuum or in counter-diffusion experiments. However, they are not relevant under the chosen experimental conditions, i.e. small gas phase pressures ($<10^3$ Pa) and slow desorption rate of the desorbing component.

We have already demonstrated in a previous work that external mass transfer resistances created by release of heat of adsorption are negligible in our experiments with individual crystals [29]. This marks another important advantage over setups running with crystal batches or self-supporting wafers.

The details of the CBMC simulations of adsorption equilibrium are given in the Supplementary material accompanying this paper.

The silicalite-1 crystals were synthesized by W. Schmidt (Mülheim). Details of synthesis and characterization of the silicalite-1 crystals used in this study are given elsewhere [30]. The activation procedure and more information on the structure are given in the Supplementary material.

Silicalite-1 belongs to zeolites with MFI-type structure. The channel network consists of mutually intersecting straight and zigzag channels with a cross-section of about 5.5 Å (see Fig. 1).

One unit cell includes four intersections, four straight and four zigzag channel segments. The crystals are internally twinned forming a 90° intergrowth structure as proven by disintegration of the crystals segments [30]. The crystallographic axis of two adjacent

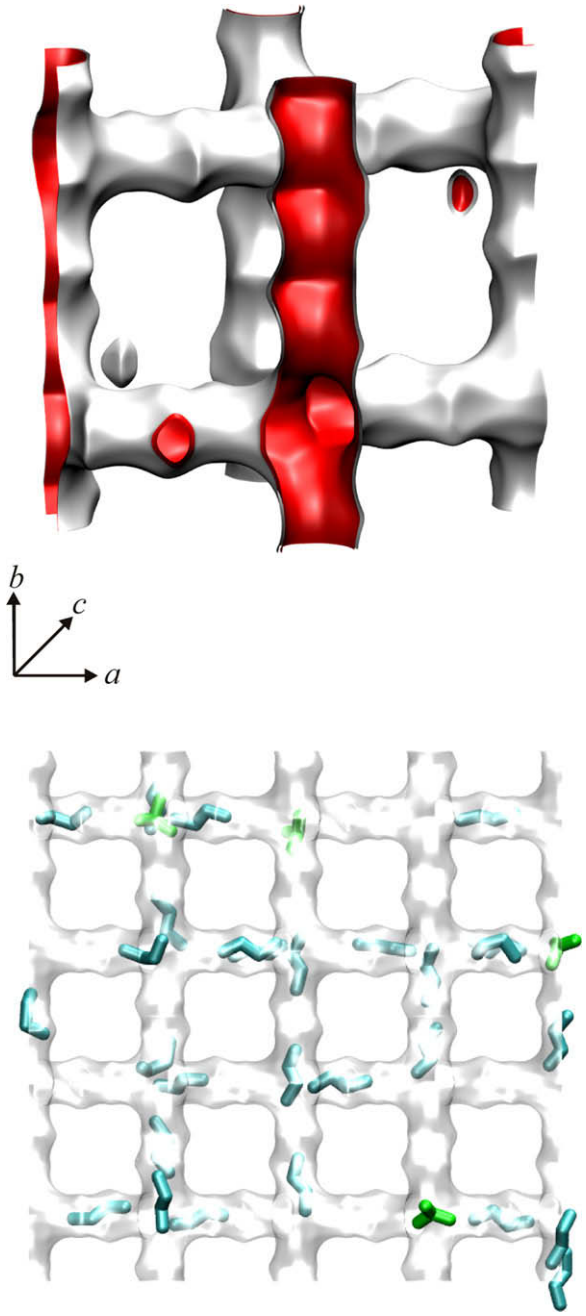

Fig. 1. Schematic representation of the MFI channel network. The sinusoidal channels run along crystallographic *a*, straight channels along *b* direction. Also shown are snapshots of the location of nC4 and iC4 within the straight and zigzag channels of silicalite-1.

segments is rotated by 90° around the *c*-axis. The openings of the straight channels lead to the internal interfaces. Only the sinusoidal channels have access to the outer surface of these segments and, consequently, the transport in these crystals occurs predominantly along the zigzag channels in our experiments.

3. Adsorption isotherms

Adsorption isotherms are required to relate the intracrystalline loading with the pressure in the gas phase surrounding the crystals. Single component isotherms of iC4 in individual silicalite-1 crystals were measured with IRM. The experimental data were found to be in excellent agreement with results of CMBC simulations as presented in Refs. [25,31]. It is important to note that the iC4 molecules are preferably located at the channel intersections. This gives rise to an inflection in the iC4 isotherm at a loading of 4 molecules per unit cell when all intersections are occupied [25,32]. The comparison between IRM data and the CBMC isotherm for nC4 is shown in the Supplementary material of this paper. Again, experiments and simulations show excellent agreement.

The component loadings in a gas mixture can differ dramatically from the loading found for single components. For interpretation of the results presented later, the equilibrium isotherm for a 50:50 mixture of nC4–iC4 in the gas phase has been considered in CBMC simulations. Fig. 2 shows the comparison of single component and mixture loadings for identical partial pressures.

The nC4 loading in mixture is reduced by about 15% but follows essentially a similar trend as the single-component isotherm. However, the concentration of iC4 in the mixture is not only severely reduced, but remains practically constant for pressures higher than 100 Pa. This dependence is probably related to the effects of 'configurational entropy' as discussed in [33]. nC4 can simply 'pack' more efficiently than iC4 in the MFI channel network and is, hence, favoured in mixture adsorption. The CBMC isotherms are compared with experimental data of IRM at different loadings in Fig. 2. The IR data were calibrated using the CBMC isotherm to determine the absolute loading in the IR experiments. In the considered range the agreement between experiments and simulations is nearly perfect.

4. Results of mixture-diffusion measurements

Transport in mixtures is determined by an interplay of various factors and is usually a complex function of, i.e. adsorption strength, fractional occupancy and mutual influence and correlation effects of the components [3,34,35]. It has been demonstrated that, based on an exact knowledge of single-component adsorption and diffusivities, the mixture diffusivities can be quantitatively predicted employing Maxwell–Stefan theory [36–38]. However, in order to derive the main conclusions presented here it is sufficient to attempt a qualitative interpretation of the experimental results.

For understanding the mixture uptake data it is important to recapitulate that iC4 prefers to occupy intersection sites. Already single-component diffusion of iC4 is strongly influenced by this preference. The transport diffusivity, i.e. Fick diffusivity, increases strongly for loadings higher than 4 molecules per unit cell, when all intersection sites are filled. Furthermore, the Maxwell–Stefan diffusivity exhibits a sharp minimum at this loading, with a cusp-shaped loading dependence [25].

The mobility of nC4 in MFI crystals is about two orders of magnitude higher than that of iC4. It has already been shown that the self-diffusivity of nC4 is sharply reduced, if a certain fraction of these traffic junctions is 'blocked' by the much more immobile iC4 [5]. Moreover, the diffusivity of linear alkanes in MFI-type zeolites seems to be severely reduced in general in presence of increased amounts of branched and cyclic hydrocarbons due to this intersection blocking [24].

Concerning the mixture-diffusion measurements under non-equilibrium conditions, we shall consider the influence of the initial iC4 loading on "counter-uptake" of nC4 at first. The impact on transport of nC4 was measured for five different initial iC4 loadings between 0 and 4.0 molecules per unit cell (Fig. 3). The equilibrium loading of iC4 was almost zero. That of nC4 was approximately 6.4 molecules per unit cell in all cases, considerably larger than the initial iC4 concentration. Two characteristic features can be noted: (i) the nC4 uptake seems to be slowed down with increasing initial iC4 concentration, (ii) a step occurs at early times, which is the smaller the higher the initial iC4 loading is.

The exchange of iC4 by nC4 may be further analysed by looking at the partial loadings of nC4 and iC4 plotted together with the total loading (Fig. 4). Since the transfer rates of both molecules are

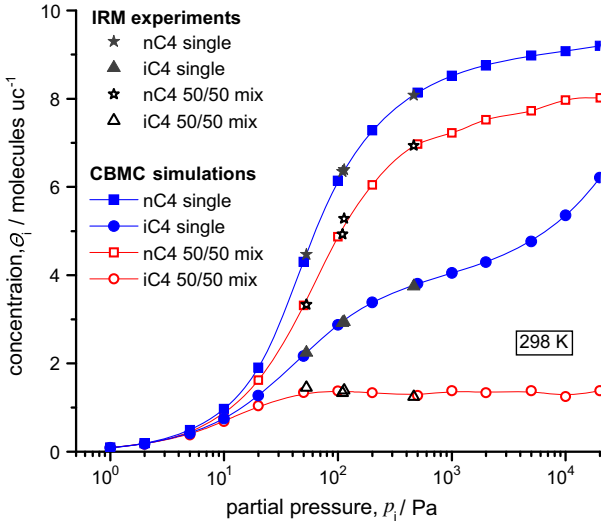

Fig. 2. CBMC isotherms for single components (connected full symbols) and 50:50 gas mixture (connected open symbols) of nC4 and iC4 in silicalite-1. The simulations are compared with experimental results obtained by IRM (full symbols – single component, open symbols – mixture).

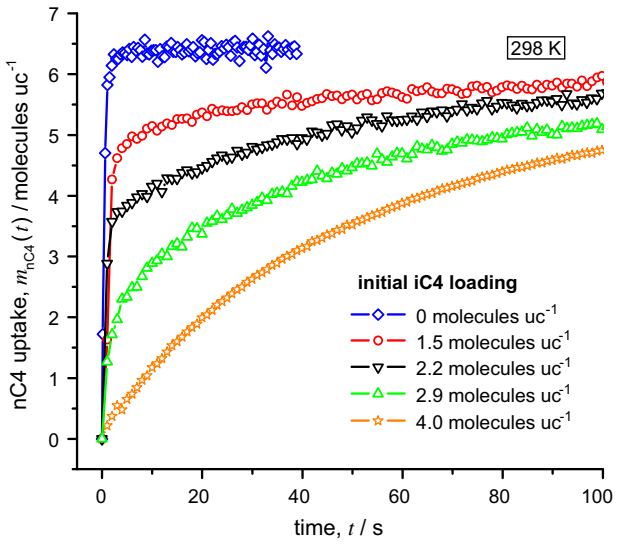

Fig. 3. Impact of different initial iC4 loadings on the 'counter-uptake' of nC4. The rate of nC4 is determined by the availability of free sites, i.e. by the release of iC4.

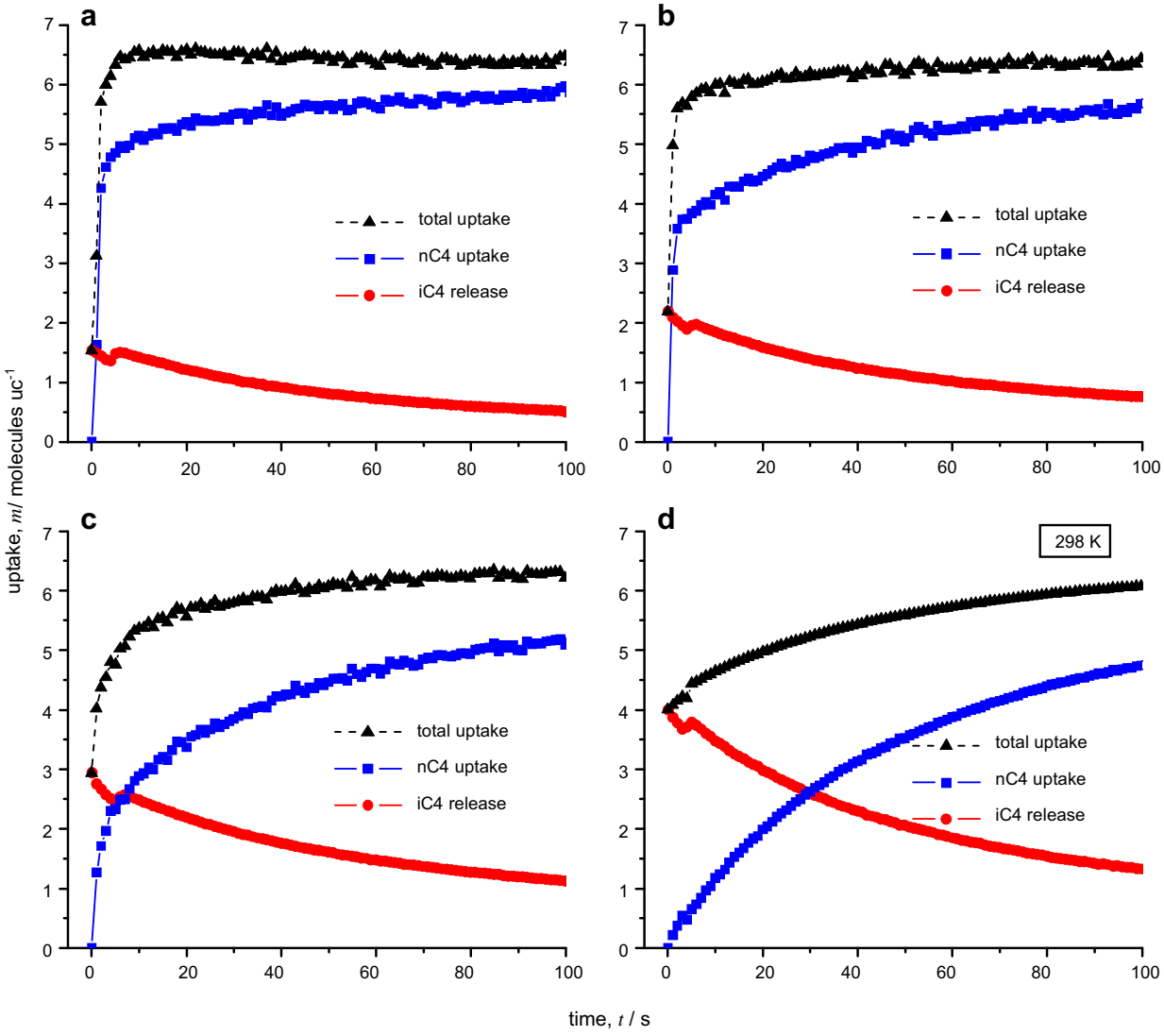

Fig. 4. Counter-uptake of nC4 under presence of iC4 at initial concentrations of: (a) 1.5, (b) 2.2, (c) 2.9 and (d) 4.0 molecules per unit cell, respectively. The partial loadings (square and circle symbols) are plotted along with the total loading (triangles).

very different the exchange process can be understood as a 2-step process. First, nC4 promptly occupies all adsorption places which are accessible from the outer surface, according to the equilibrium value. As a second step, iC4 slowly desorbs, vacating new adsorption sites accessible for nC4.

These vacated sites have been directly occupied or belong to regions shielded by iC4. The number of shielded sites is strongly correlated with the concentration of iC4. In this respect the pore structure of MFI-type is similar to the diamond structure, so a site percolation threshold of 0.43 may be assumed to describe the influence of iC4 [39]. This corresponds to an iC4 loading of 2.3 molecules uc^{-1}. It has to be stated that even for concentrations below the percolation threshold, some unoccupied sites are shielded by iC4. For loadings in the region of the percolation threshold, the area of the shielded regions increases significantly with concentration. Furthermore, the length of unblocked diffusion path segments for nC4 decreases with increasing iC4 concentration resulting in a significantly reduced nC4 transfer rate, even if it still could percolate through the crystal. On the other hand, this threshold describes the percolation of a lattice with immobile molecules at the intersections. In reality, however, the molecules diffuse which shifts the threshold towards higher loadings. So, the percolation threshold may be used to roughly describe the correlation between the nC4 diffusion and the iC4 concentration.

In the first case (Fig. 4a), the initial iC4 concentration is 1.5 which is below the percolation threshold. nC4 occupies instantaneously the unoccupied sites and the number of nC4 molecules adsorbing in the second step equals the number of desorbing iC4 molecules. This means there are no shielded sites and the overall concentration remains practically constant during the second step of the exchange process.

In the range of the percolation threshold, the number of sites which are directly accessible from the outer surface decreases with increasing iC4 concentration (Fig. 4b and c). This results in an nC4 concentration which increases stronger than the iC4 concentration decreases, i.e. the overall concentration increases during the second step.

Finally, when all junctions are initially occupied by iC4 (Fig. 4d), there are no adsorption sites accessible from the outer surface. Hence, the first step of the exchange process cannot be observed. And, consequently, the uptake of nC4 is limited by the release of iC4 during the whole exchange process.

This behaviour may also be visualized by plotting the difference between the final and the actual loading versus time (Fig. 5). In the

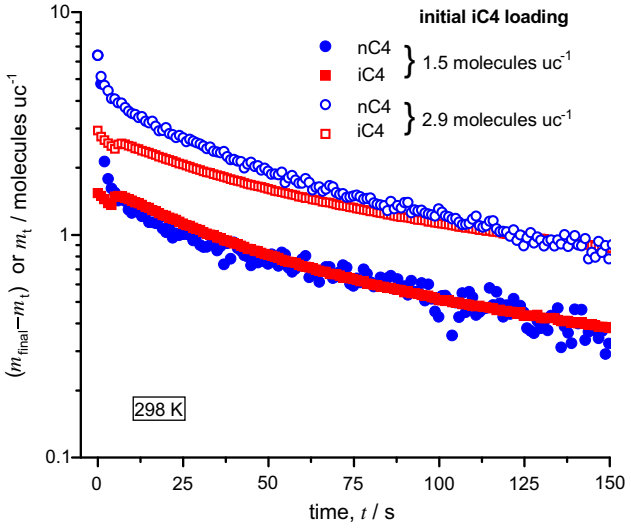

Fig. 5. Time dependence of the difference between the final and the actual loading for counter-uptake of nC4 at two different initial iC4 loadings.

case where no adsorption sites are shielded by iC4 (initial iC4 loading 1.5 molecules per unit cell) the release of iC4 and the uptake of nC4 show coinciding data during the entire second step. If there exist some regions of the network which are initially shielded by iC4 (initial iC4 loading 2.9 molecules per unit cell), a difference between both signals is observed since nC4 fills more sites than vacated by iC4. Only for long times both curves coincide. As general conclusion we find, that the nC4 uptake is not limited by diffusion but by the availability of free sites.

Now, we consider so called co-adsorption experiments. Since the nC4 equilibrium loading is reached within the first seconds, the iC4 uptake may also be described as uptake under the presence of nC4. Single component and mixture uptake curves for nC4 and iC4 at similar partial gas phase pressures are compared in Fig. 6. The following loading steps are covered: nC4 single uptake 0–6.4 molecules uc^{-1}, nC4 in mixture 0–5.0 molecules uc^{-1}, iC4 single uptake 0–2.9 molecules uc^{-1} and iC4 in mixture 0–1.4 molecules uc^{-1}.

For the considered step the nC4 uptake is unaffected by the presence of iC4 within the experimental uncertainty. Concerning

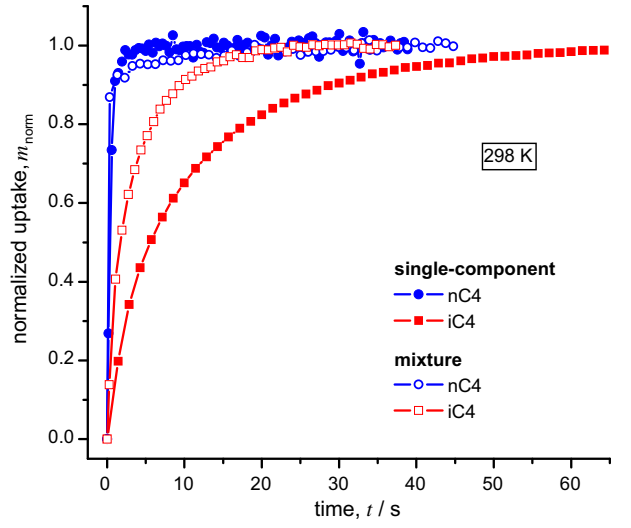

Fig. 6. Comparison of single-component (filled symbols) and mixture uptake (open symbols) of nC4 and iC4.

the iC4 equilibrium mixture loading of 1.4 molecules uc^{-1}, the reduction of the nC4 uptake rate can be estimated to be smaller than a factor of 2. Probably, the uptake must be recorded with higher time-resolution to resolve this effect in the mixture uptake curve.

The iC4 uptake in presence of nC4 is found to be increased by a factor of about 2.5. This might be explained with a higher transport rate at the higher total loading in the mixture case. In single-component experiments a strong increase of the diffusivity was found for loadings higher than 4 molecules uc^{-1}, which could be related to a decrease in the energy barrier for jumps between adjacent sites due to inter-molecular repulsions [25]. A similar argument might hold for the increased iC4 uptake rate under presence of nC4 (Fig. 6). It could be an attractive and challenging task for a future work to investigate this effect in detail striving for a quantitative description, in particular since it may have further implications for applications in membrane processes or catalysis. One can speculate, e.g. that inter-molecular repulsions are responsible for the reduced separability of an nC4/iC4 mixture for increasing transmembrane pressures through a siliclalite-1 membrane, as reported and discussed in another work of this special issue [40].

5. Conclusion

Adsorption and diffusion of *n*-butane/*iso*-butane mixtures in individual silicalite-1 crystals has been investigated using IR microscopy and computer simulations.

The experimental data of the equilibrium sorption isotherm have been found to be in excellent agreement with the isotherm obtained from CBMC simulations. The simulation results could be used to calibrate the IR data enabling the determination of absolute concentration in the experiments.

The *n*-butane counter-uptake under presence of *iso*-butane has been investigated for different initial *iso*-butane loadings between zero and 4 molecules per unit cell. The *n*-butane uptake was found to be limited by the availability of free sites rather than the *n*-butane diffusivity. The availability of free sites in turn, is determined by the rate at which *iso*-butane desorbs from the crystal.

The large difference in the diffusivity by about two orders of magnitude implicates that the much more immobile *iso*-butane is able to "shield" network regions from *n*-butane by occupying and blocking channel intersections, which act as preferred sites for *iso*-butane. A site-percolation threshold given by the number of *iso*-butane molecules blocking these 'traffic junctions' has been found to nicely describe the fraction of network regions which are initially inaccessible for *n*-butane.

The reported work is relevant not only in the modelling and design of zeolite membrane permeation processes, but also for catalytic processes in which one of the reactants (such as *iso*-alkanes, or benzene) is located preferentially at the intersections of MFI-type crystals [41].

Acknowledgments

We dedicate this paper to Professor Jörg Kärger on the occasion of his 65th birthday. The authors, especially CC and LH, owe a special debt of gratitude to Professor Kärger for numerous stimulating and fruitful scientific, cultural and human exchange, for collaboration in many successful projects for his excellent support, supervision and guidance.

We are obliged to Wolfgang Schmidt for synthesizing and providing the zeolite crystals. We also want to thank Dhananjai B. Shah for some help related with the experiments.

Financial support by *Deutsche Forschungsgemeinschaft* (Mercator Professorship for RK, International Research Group "Diffusion in

Zeolites" and International Research Training Group "Diffusion in Porous Materials"), *European Union* (NoE INSIDE POReS), *Studienstiftung des deutschen Volkes* and *Fonds der Chemischen Industrie* is gratefully acknowledged.

Appendix A. Supplementary data

Supplementary data associated with this article can be found, in the online version, at doi:10.1016/j.micromeso.2009.02.015.

References

[1] J. Kärger, M. Bülow, P. Lorenz, J. Colloid Interface Sci. 65 (1978) 181.
[2] J. Caro, M. Bülow, J. Richter-Mendau, J. Kärger, M. Hunger, D. Freude, L.V.C. Rees, J. Chem. Soc. Faraday Trans. I 83 (1987) 1843.
[3] J. Kärger, D.M. Ruthven, Diffusion in Zeolites and Other Microporous Solids, Wiley & Sons, New York, 1992.
[4] R.Q. Snurr, J. Kärger, J. Phys. Chem. B 101 (1997) 6469.
[5] M. Fernandez, J. Kärger, D. Freude, A. Pampel, J.M. van Baten, R. Krishna, Micropor. Mesopor. Mat. 105 (2007) 124.
[6] F. Schüth, K.S.W. Sing, J. Weitkamp (Eds.), Handbook of Porous Materials, Wiley-VCH, Weinheim, Germany, 2002.
[7] U. Schemmert, J. Kärger, J. Weitkamp, Micropor. Mesopor. Mater. 32 (1999) 101.
[8] J. Kärger, P. Kortunov, S. Vasenkov, L. Heinke, D.B. Shah, R.A. Rakoczy, Y. Traa, J. Weitkamp, Angew. Chem. Int. Ed. 45 (2006) 7846.
[9] L. Heinke, P. Kortunov, D. Tzoulaki, J. Kärger, Phys. Rev. Lett. 99 (2007) 228301.
[10] L. Heinke, J. Kärger, New J. Phys. 10 (2008) 023035.
[11] H.G. Karge, J. Weitkamp, Chemie-Ingenieur-Technik 58 (1986) 946.
[12] H.G. Karge, W. Niessen, Catal. Today 8 (1991) 451.
[13] W. Nießen, H.G. Karge, Micropor. Mesopor. Mat. 1 (1993) 1.
[14] H.G. Karge, C.R. Chimie 8 (2005) 303.
[15] S. Jost, N.K. Bär, S. Fritzsche, R. Haberlandt, J. Kärger, J. Phys. Chem. B 102 (1998) 6375.
[16] L.N. Gergidis, D.N. Theodorou, H. Jobic, J. Phys. Chem. B 104 (2000) 5541.
[17] D. Schuring, A.O. Koriabkina, A.M. de Jong, B. Smit, R.A. van Santen, J. Phys. Chem. B 105 (2001) 7690.
[18] E.R. Geus, H. van Bekkum, W.J.W. Bakker, J.A. Moulijn, Micropor. Mat. 1 (1993) 131.
[19] J. Coronas, R.D. Noble, R.D. Falconer, Ind. Eng. Chem. Res. 37 (1998) 166.
[20] D.M. Ruthven, in: J. Kärger (Hrsg.), Leipzig, Einstein Diffusion, Leipziger Universitätsverlag, Leipzig, Germany, 2007, p. 123.
[21] M. Schenk, S.L. Vidal, T.J.H. Vlugt, B. Smit, R. Krishna, Langmuir 17 (2001) 1558.
[22] J.F. Denayer, G.V. Baron, J.A. Martens, P.A. Jacobs, J. Phys. Chem. B 102 (1998) 3077.
[23] R. Krishna, B. Smit, T.J.H. Vlugt, J. Phys. Chem. A 102 (1998) 7727.
[24] R. Krishna, J.M. van Baten, Chem. Eng. J. 140 (2008) 614.
[25] C. Chmelik, L. Heinke, J. Kärger, W. Schmidt, D.B. Shah, J.M. van Baten, R. Krishna, Chem. Phys. Lett. 459 (2008) 141.
[26] C. Chmelik, J. Kärger, M. Wiebcke, J. Caro, J.M. van Baten, R. Krishna, Micropor. Mesopor. Mater. 117 (2009) 22.
[27] M. Bülow, J. Kärger, M. Kočiřík, M. Voloscuk, Z. Chem. 21 (1981) 175.
[28] V. Masařík, P. Novák, A. Zikánová, J. Kornatowski, J. Maixner, M. Kočiřík, Coll. Czech. Chem. Commun. 63 (1998) 321.
[29] L. Heinke, C. Chmelik, D.B. Shah, S. Brandani, D.M. Ruthven, J. Kärger, Micropor. Mesopor. Mater. 104 (2007) 18.
[30] W. Schmidt, U. Wilczok, C. Weidenthaler, O. Medenbach, R. Goddard, G. Buth, A. Cepak, J. Phys. Chem. B 111 (2007) 13538.
[31] C. Chmelik, A. Varma, L. Heinke, D.B. Shah, J. Kärger, F. Kremer, U. Wilczok, W. Schmidt, Chem. Mater. 19 (2007) 6012.
[32] R. Krishna, D. Paschek, Phys. Chem. Chem. Phys. 3 (2001) 453.
[33] R. Krishna, B. Smit, S. Calero, Chem. Soc. Rev. 31 (2002) 185.
[34] J. Kärger, Surf. Sci. 36 (1973) 797.
[35] Y. Wang, M.D. Le Van, J. Phys. Chem. B 112 (2008) 8600.
[36] R. Krishna, D. Paschek, Phys. Chem. Chem. Phys. 4 (2002) 1891.
[37] R. Krishna, Chem. Phys. Lett. 355 (2002) 483.
[38] R. Krishna, J.M. van Baten, Chem. Eng. Sci. 63 (2008) 3120.
[39] J. Holakovský, I. Kratochvílová, M. Kočiřík, Micropor. Mesopor. Mat. 91 (2006) 170.
[40] J. Caro, Micropor. Mesopor. Mat. 125 (2009) 79.
[41] N. Hansen, R. Krishna, J.M. van Baten, A.T. Bell, F.J. Keil, J. Phys. Chem. C 113 (2009) 235.

Supplementary material to accompany:

Diffusion of *n*-butane/*iso*-butane mixtures in silicalite-1 investigated using infrared (IR) microscopy

C. Chmelik[(1)], *L. Heinke*[(1)], *J.M. van Baten*[(2)] *and R. Krishna*[(2)]

[(1)] Department of Interface Physics, University of Leipzig, Linnéstrasse 5, D-04103 Leipzig, Germany

[(2)] Van 't Hoff Institute for Molecular Sciences, University of Amsterdam, Nieuwe Achtergracht 166, 1018 WV Amsterdam, The Netherlands

Appendix A1:

Silicalite-1 structure and activation procedure

1. Silicalite-1 structure

Silicalite-1 or ZSM-5 are the most prominent representatives of MFI-type zeolites. The 5-1 secondary building units of these crystalline aluminosilicates consist of AlO_4- and SiO_4 tetrahedra linked by oxygen bridges. Silicalite-1 is defined to have a Si/Al ratio of larger than 1000. MFI-type zeolites have a three-dimensional connected pore system of straight channels in *b*-direction [010], which are cross-linked by sinusoidal channels in *a*-direction [100] (see Figure 1 of the main paper). Mass transport along the *c*-direction [001] can proceed only by an alternating use of the straight and sinusoidal channels. The cross-section of the straight channels is $5.3\times5.6\,Å^2$ and $5.1\times5.5\,Å^2$ for the sinusoidal channels. The unit cell parameters are a = 20.07 Å, b = 19.74 Å and c = 13.14 Å [1,2]. The straight segments have a length of 9.95 Å and the zig-zag segments a length of 12.07 Å, if measured from one intersection centre to the next [3].

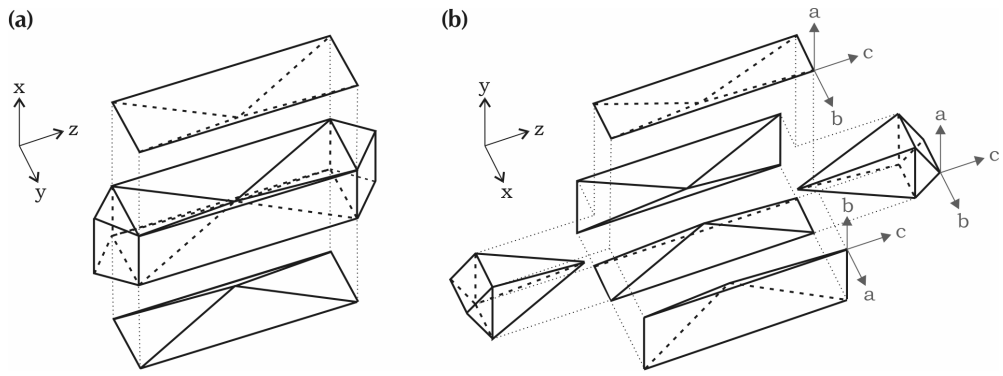

Figure 1. Models of internal structure of MFI-type crystals described in literature: (a) according to [4,8,11] and (b) to [12]. The indicated orientation of the fragments in (b) was taken form [10].

The existence of an internal twinning of MFI-type crystals is discussed in the literature since about 25 years [4]. Many papers have been published about the nature, origin and possible effects of the internal structure, but only a few show the influence on molecular transport directly [5-8]. An overview of the main conclusions of many papers on this topic is given in [6]. Two models of internal structure are discussed (see Figure 1). It is generally assumed, that only the sinusoidal channels point towards the outer surface, i.e. that a 90° intergrowth exists between the components. Consequently, the openings of the straight channels lead only to the internal interfaces. In a recent paper using interference microscopy it was shown, that in the case of *iso*-butane as guest molecule these interfaces may act as weak internal transport barriers in silicalite-1 crystals [5]. In contrast, for the material studied here, in interference microscopy investigations also with *iso*-butane, no indications for the existence of such internal barriers were found [9]. On the other hand, there are also results

published where, e.g. with iodine as a guest, the opposite may be true, viz. that fast uptake via the internal interfaces is possible [8].

Agger et al. even claim to have evidence, that there exists no intergrowth structure at all. They explain the hourglass feature as a result of differences in the refractive index in different parts of the crystal caused by different silanol group concentration [6]. Finally, in a recent work silicalite-1 crystals could be split up into the fragments by a physico-chemical treatment [10]. The fragments were created from the same material as used for the present study. Single crystal X-ray analyses proved the remaining fragments as perfect "single crystals" and showed, that only the sinusoidal channels have openings on the quadrangular faces of the large prisms and, consequently, a 90° intergrowth indeed exists for these crystals (Figure 1). Hence, the published results emphasise, that there might be no general, uniform structure of MFI-type crystals and only a careful investigation will show, which internal crystal features exist.

As another anomaly of the internal structure, in the literature also the existence of "microdomains" has been described [13]. The spatial resolution of FTIR microscopy is not sufficient to measure a possible influence of 2 - 3 µm sized microdomains directly. However, in PFG NMR studies with *n*-butane on the present material, no evidence for the existence of such internal barriers were found [14].

2. Activation procedure

For activation, several crystals were introduced in the IR cell and heated under vacuum ($< 10^{-5}$ mbar) with a heating rate of 1 K·min^{-1}. Then, the crystals were kept at a temperature of 723 K for 24 h. In addition, a calcination step under presence of oxygen was attached for about 2 h, to remove possibly existing coked organic residuals. Subsequently, the crystals were again exposed to vacuum for 3 h. After cooling the crystals to room temperature the sorption experiments were started.

References A1

[1] Ch. Baerlocher and L.B. McCusker, Database of Zeolite Structures: http://www.iza-structure.org/databases/ .

[2] Ch. Baerlocher, W.M. Meier and D.H. Olson, Atlas of Zeolite Framework Types; 5th revised edition, Elsevier, Amsterdam, 2001.

[3] R. Krishna, D. Paschek, Phys. Chem. Chem. Phys. 3 (2001) 453.

[4] G.D. Price, J.J. Pluth, J.V. Smith, J.M. Bennett, R.L. Patton, J. Am. Chem. Soc. 104 (1982) 5971.

[5] O. Geier, S. Vasenkov, E. Lehmann, J. Kärger, U. Schemmert, R.A. Rakoczy, J. Weitkamp, J. Phys. Chem. B 105 (2001) 10217.

[6] J.R. Agger, N. Hanif, C.S. Cundy, A.P. Wade, S. Dennison, P.A. Rawlinson, M.W. Anderson, J. Am. Chem. Soc. 125 (2003) 830.

[7] D.G. Hay, H. Jaeger, K.G. Wilshier, Zeolites 10 (1990) 571.

[8] M. Kočiřík, J. Kornatowski, V. Masařík, P. Novák, A. Zikánová, J. Maixner, Microporous Mesoporous Mat. 23 (1998) 295.

[9] D. Tzoulaki, L. Heinke, W. Schmidt, U. Wilczok, J. Kärger, Angew. Chem. Int. Ed. 47 (2008) 3954.

[10] W. Schmidt, U. Wilczok, C. Weidenthaler, O. Medenbach, R. Goddard, G. Buth, A. Cepak, J. Phys. Chem. B 111 (2007) 13538.

[11] C. Weidenthaler, R.X. Fischer, R.D. Shannon, O. Medenbach, J. Phys. Chem. 98 (1994) 12687.

[12] E.R. Geus, J.C. Jansen, H. van Bekkum, Zeolites 14 (1994) 82.

[13] S. Vasenkov, J. Kärger, Microporous Mesoporous Mat. 55 (2002) 139.

[14] K. Ulrich, unpublished results, Universität Leipzig, 2007.

Appendix A2:

Single component isotherm of *n*-butane and further comments on mixture diffusion results

1. Single component isotherm of *n*-butane

At the considered experimental conditions the uptake of *n*-butane proceeded very fast. E.g. sorption equilibrium was reached in less than 1 s for uptake from vacuum to 1 mbar. The fast uptake gave access to a special type of measurement, viz. to a high-resolution sorption isotherm. For such an experiment, after starting a time resolved measurement, the pressure is increased slowly but continuously. Due to the fast uptake, the system is then still in sorption equilibrium at all times. By correlating pressure with time, the sorption isotherm can be calculated (see Figure 2). To exclude a shift in the measured sorption capacity which might be caused by a heating of the crystal due to the continuous release of heat of adsorption, the pressure was kept constant at certain pressures for about 1 min. The constancy of the measured absorbance can be considered as proof, that the described heating of the crystal is negligible small.

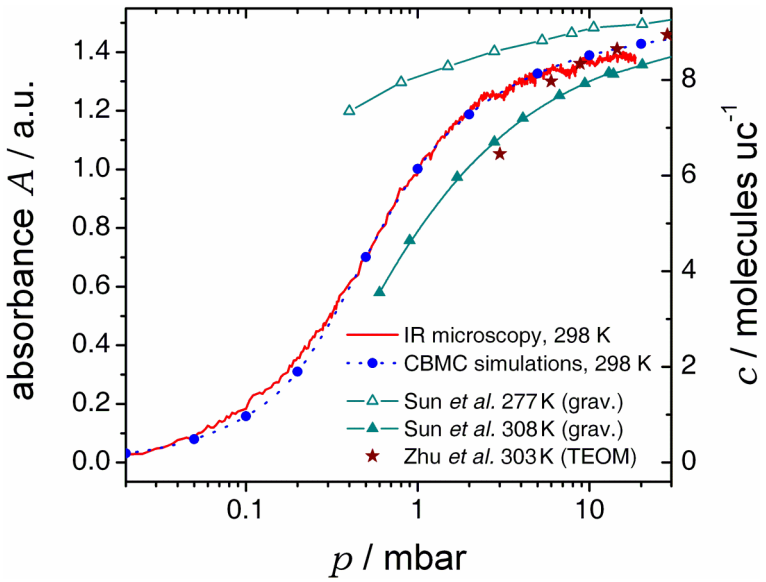

Figure 2. Adsorption isotherm of *n*-butane in silicalite-1. Correlation of high-resolution IR data with results of CBMC simulations to determine the intracrystalline concentration. For comparison other literature data are also shown [15, 16].

In analogy to *iso*-butane [17], the IR data were compared with the results of Configurational Bias Monte-Carlo simulations to obtain the *n*-butane loading in absolute units. The agreement between both data sets is excellent (Figure 2). In addition, literature data for isotherms measured at comparable temperatures are re-plotted. The isotherm measured gravimetrically by *Sun et al.* for 308 K [16] follows practically the same trend but is shifted somewhat to lower loadings. The lower loading is a result of the reduced sorption equilibria due to the by 10 K higher environmental temperature. The agreement with results of *Zhu et al.*

for 303 K obtained by using a tapered element oscillating microbalance (TEOM) device [15] is acceptable.

Compared to the other experimental data two main advantages of the high-resolution isotherm measurement can be noted. First, the isotherm is measured with a very high resolution. In the present case about 650 points were recorded between 0.01 mbar and 18.5 mbar within a time of 1 h. Second, the isotherm can be recorded also in the low pressure region with high accuracy. However, the use is limited to systems with fast equilibration times.

2. Further comments on mixture diffusion results

The reader might find it interesting to compare the findings of the main paper with results presented in ref. [18]. However, it has to be taken into account, that the uptake in the IRM experiments proceeds mainly along the zigzag channels, whereas for PFG NMR an average of the diffusivity in all crystallographic directions is measured. In this respect it is important to note that the drop in the *n*-butane self-diffusivity at about 2 molecules per unit cell results mainly from the reduced diffusivity along the straight channels. For transport along the straight channels the drop in the mobility is expected to occur significantly below the percolation threshold.

The results of MD simulations predict for several alkanes that the diffusivity along the straight channels is by about 2-3 times larger than in the direction of the zigzag channels [19-21]. Considering the number of connected straight channel segments without enclosed occupied intersections, one may easily follow the argument that this anisotropy for diffusion along the straight and zigzag channels (i.e. faster diffusion along the straight channels) may cancel out if more than 1/3 of the intersections are blocked by *iso*-butane. Due to the 90° intergrowth such considerations can be neglected for the IRM mixture experiments.

Some comments on the consequence of the 90° intergrowth on single-component uptake are also included in the supplementary material to ref. [17].

References A2

[15] W. Zhu, F. Kapteijn and J.A. Moulijn; *Phys. Chem. Chem. Phys.* **2** (2000) 1989–1995.

[16] M.S. Sun, D.B. Shah, H.H. Xu and O. Talu; *J. Phys. Chem. B* **102** (1998) 1466–1473.

[17] C. Chmelik, L. Heinke, J. Kärger, W. Schmidt, D.B. Shah, J.M. van Baten, R. Krishna, Chem. Phys. Lett. 459 (2008) 141.

[18] M. Fernandez, J. Kärger, D. Freude, A. Pampel, J.M. van Baten, R. Krishna, Micropor. Mesopor. Mat. 105 (2007) 124.

[19] E.B. Webb III, G.S. Grest, M. Mondello, J. Phys. Chem. B 103 (1999) 4949.

[20] A. Bouyermaouen, A. Bellemans, J. Chem. Phys. 108 (1998) 2170.

[21] T.J.H. Vlugt, C. Dellago, B. Smit, J. Chem. Phys. 113 (2000) 8791.

Appendix A3:

Molecular Simulation methodology and results

1. CBMC simulations

Configurational-Bias Monte Carlo (CBMC) simulations have been carried out to determine the adsorption isotherms for pure component *n*-butane (nC4), and *iso*-butane (iC4), along with nC4-iC4 mixtures in MFI (all silica silicalite-1) at 298 K; the crystallographic data are available elsewhere [22,23].

We use the united atom model. The zeolite framework is considered to be rigid. We consider the CH_x groups as single, chargeless interaction centers with their own effective potentials. The beads in the chain are connected by harmonic bonding potentials. A harmonic cosine bending potential models the bond bending between three neighboring beads, a Ryckaert-Bellemans potential controls the torsion angle. The beads in a chain separated by more than three bonds interact with each other through a Lennard-Jones potential. The Lennard-Jones potentials are shifted and cut at 12 Å. The CBMC simulation details, along with the force fields have been given in detail in earlier publications [24,25]. The simulation box consists of 2×2×4 unit cells for MFI. Periodic boundary conditions were employed. It was verified that the size of the simulation box was large enough to yield reliable data on adsorption.

The CBMC simulations were performed using the BIGMAC code developed by T.J.H. Vlugt [26] as basis. The code was modified to handle rigid molecular structures and charges. S. Calero is gratefully acknowledged for her technical inputs in this regard.

The CBMC simulations of the adsorption isotherms for pure nC4, and pure iC4 in MFI at 298 K are presented in Figure 1. The continuous solid lines in Figures 1 are dual-site Langmuir fits of the isotherm

$$\Theta = \frac{\Theta_{sat,A} b_A p}{1 + b_A p} + \frac{\Theta_{sat,B} b_B p}{1 + b_B p} \quad . \tag{1}$$

The values of the fitted parameters b and Θ_{sat} are specified in Table 1.

Figure 2 shows the mixture adsorption isotherms for nC4 and iC4 in MFI at 298 K obtained from CBMC simulations.

Snapshots showing the location of the nC4 and iC4 molecules at different component loadings in the mixture are shown in Figures 3, 4, and 5. Note that the views in these snapshots are 2 unit cells deep.

Table 1. Dual-site Langmuir parameters for nC4 and iC4 in MFI at 298 K. The saturation capacity, q_{sat}, has the units of molecules per unit cell. The Langmuir parameters, b, have the units of Pa^{-1}.

	b_A	$\Theta_{sat,A}$	b_B	$\Theta_{sat,B}$
nC4	1.48×10^{-5}	1	1.2×10^{-2}	9
iC4	2.4×10^{-2}	4	2.85×10^{-5}	6

References A3

[22] C. Baerlocher, L.B. McCusker, Database of Zeolite Structures, International Zeolite Association, http://www.iza-structure.org/databases/, 26 June 2001.

[23] J.M. van Baten, R. Krishna, MD Simulations of Diffusion in Zeolites, University of Amsterdam, http://www.science.uva.nl/research/cr/md/,

[24] D. Dubbeldam, S. Calero, T.J.H. Vlugt, R. Krishna, T.L.M. Maesen, E. Beerdsen, B. Smit, Force Field Parametrization through Fitting on Inflection Points in Isotherms, Phys. Rev. Lett. 93 (2004) 088302.

[25] D. Dubbeldam, S. Calero, T.J.H. Vlugt, R. Krishna, T.L.M. Maesen, B. Smit, United Atom Forcefield for Alkanes in Nanoporous Materials, J. Phys. Chem. B 108 (2004) 12301-12313.

[26] T.J.H. Vlugt, BIGMAC, University of Amsterdam, http://molsim.chem.uva.nl/bigmac/, 1 November 2000.

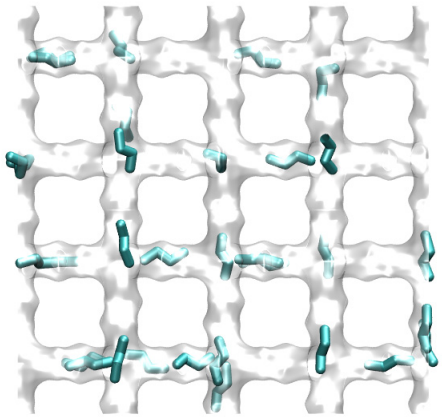

nC4 adsorbs along straight and zig-zag channels

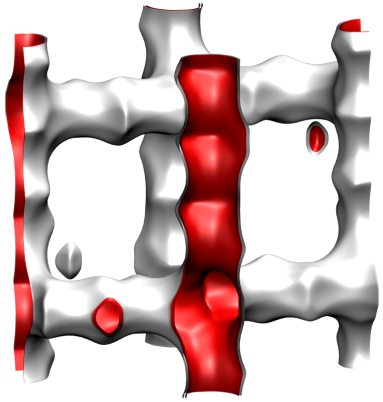

Pure component adsorption isotherms at 298 K in MFI

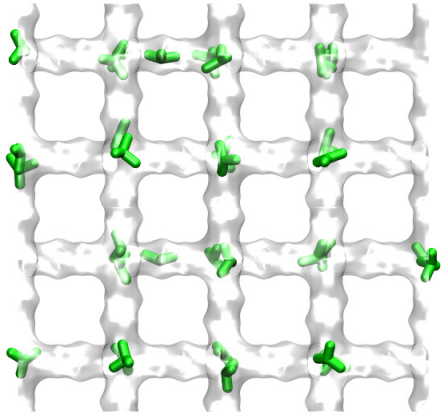

iC4 locates mainly at the intersections

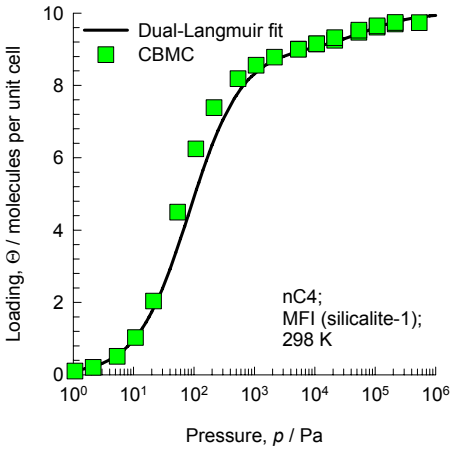

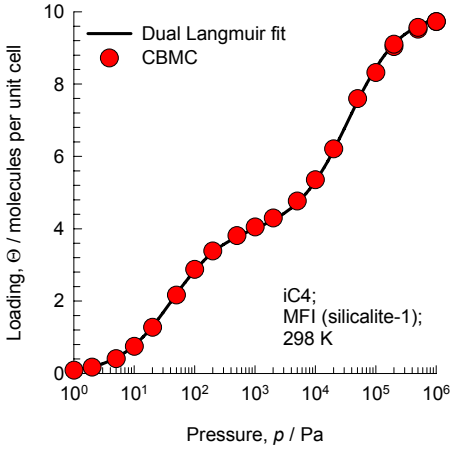

Figure 1. Pure component adsorption isotherms for nC4 and iC4 in MFI at 298 K obtained from CBMC simulations.

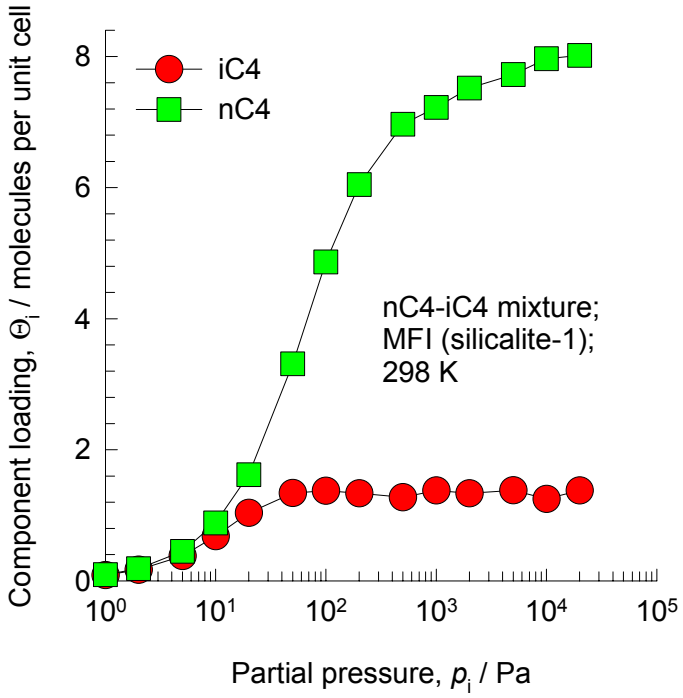

Mixture adsorption isotherm at 298 K in MFI

Figure 2. Mixture adsorption isotherms for nC4 and iC4 in MFI at 298 K obtained from CBMC simulations.

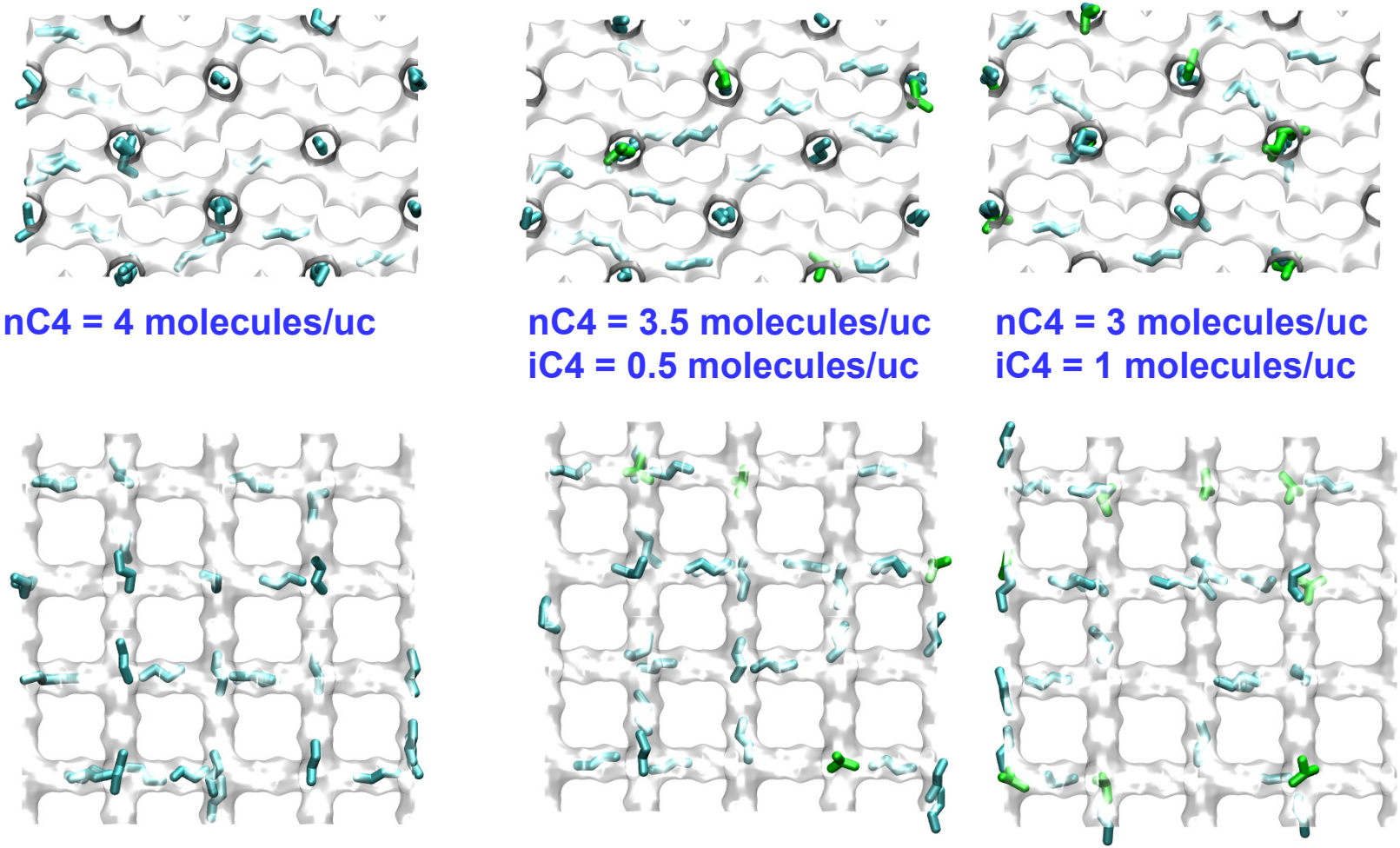

Figure 3. Snapshots showing location of nC4 and iC4 at mixture loadings (in molecules per unit cell) of (a) nC4 = 4, iC4 = 0, (b) nC4 = 3.5, iC4 = 0.5, and (c) nC4 = 3, iC4 = 1.

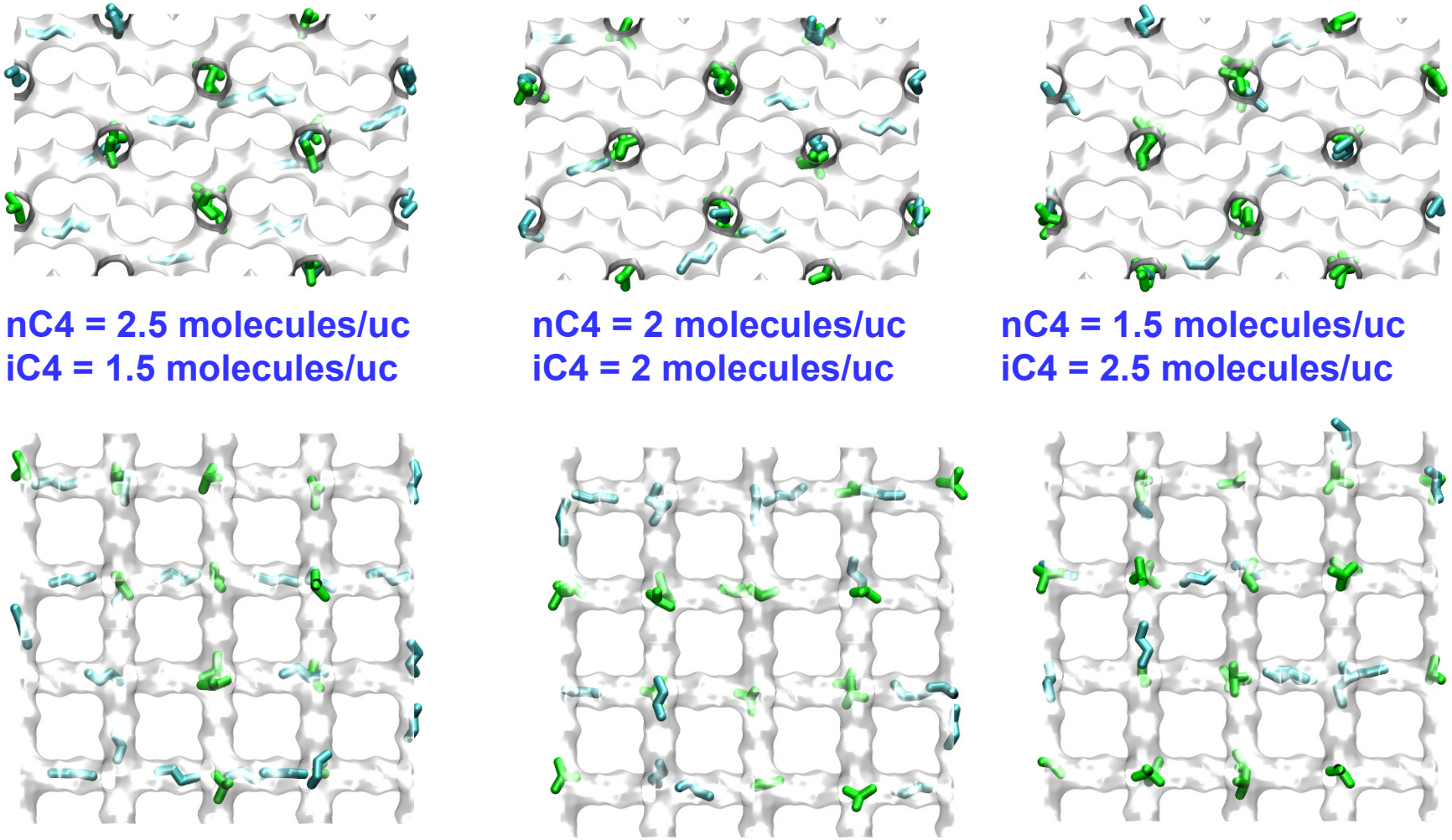

Figure 4. Snapshots showing location of nC4 and iC4 at mixture loadings (in molecules per unit cell) of (a) nC4 = 2.5, iC4 = 1.5, (b) nC4 = 2, iC4 = 2, and (c) nC4 = 1.5, iC4 = 2.5.

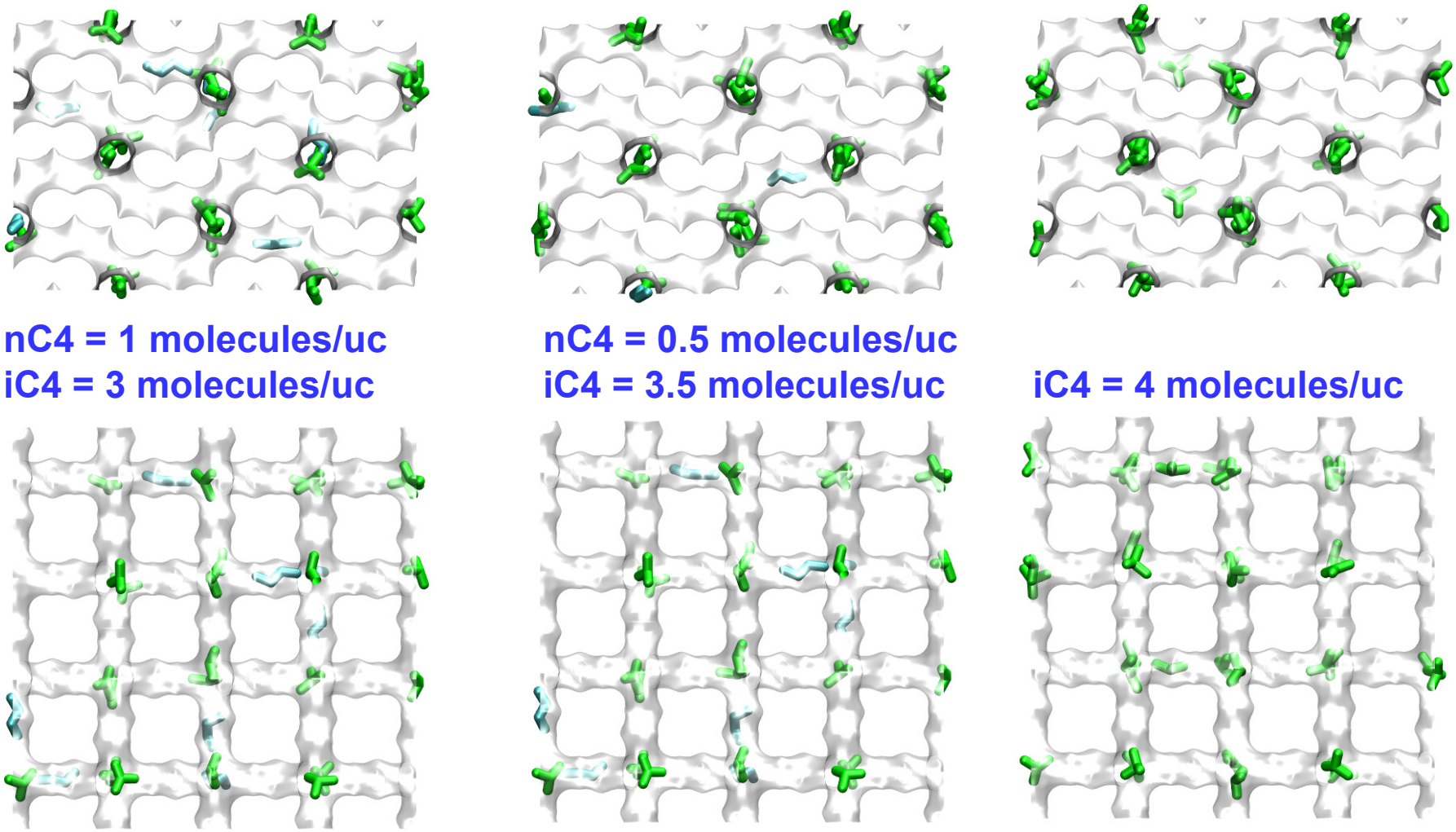

Figure 5. Snapshots showing location of nC4 and iC4 at mixture loadings (in molecules per unit cell) of (a) nC4 = 1, iC4 = 3, (b) nC4 =0.5, iC4 = 3.5, and (c) nC4 = 0, iC4 = 4.